dramatic increase of the tunneling current with increasing voltage because of tunneling through the NIR state (*21*). Based on $I(V)$ measurements for other adsorbates on NaCl films, we estimate that tunneling through the NIR state increases the tunneling current by about two orders of magnitude. The extrapolation of I to $\Delta z = 10.5$ Å and $V = 1.4$ V thus gives a current on the order of one electron per second, corresponding to a quantum yield on the order of unity. This extremely high yield is consistent with a capture of electrons tunneling into the NIR state. Further support for this interpretation comes from the experimentally suggested position of a resonance level at $E_{NIR} = 1.4$ eV above E_F or 2.6 eV below the vacuum level (*22*), which is close to the electron affinity of an isolated Au atom of 2.3 eV (below the vacuum level). Finally, for V smaller than 0.9 V, the quantum yield can be measured directly and increases exponentially with increasing voltage (Fig. 3, inset). This exponential increase is consistent with the observed linear increase of Δz at voltages well below the NIR state.

The difference in physical properties of the two states is documented in diffusion experiments. Interestingly, the two differently charged states of the Au adatom are conserved during the diffusion process. In the Au^0 state, adatom diffusion sets in at a temperature of about 60 K, whereas in the Au^- state the adatoms already diffuse at a lower temperature of 40 K. This difference even allows the diffusion of single Au adatoms to be switched on and off.

Small clusters of Au adatoms can similarly be switched between different charge states, which was demonstrated in an experiment for Au dimers and trimers on NaCl films. Nanometer-sized Au clusters on insulators have been shown to be catalytically active by partial electron transfer from color centers (*23*). This finding opens up the possibility of switching surface catalytic reactions on and off by manipulating the charge state of individual nanometer-sized Au clusters. The switching between the two differently charged states also suggests their use as a nonvolatile memory device at the ultimate spatial limit.

Associated with the control of the charge state of the Au adatom is the control of its magnetic moment. In the Au^0 adatom, the 6*s*-derived state is partially occupied, resulting in a net (spin) magnetic moment, whereas in the Au^- adatom this state is fully occupied and the adatom is nonmagnetic. This moment is expected to be paramagnetic because the magnetic-anisotropy energy of the Au(6*s*)-derived state should be minimal. However, a paramagnetic moment that is decoupled from a metal substrate by an insulating film might be of some interest in quantum-information processing.

References and Notes

1. L. C. Pauling, *The Nature of the Chemical Bond* (Cornell Univ. Press, Ithaca, NY, 1939).
2. D. M. Eigler, E. K. Schweizer, *Nature* **344**, 524 (1990).
3. D. M. Eigler, C. P. Lutz, W. E. Rudge, *Nature* **352**, 600 (1991).
4. T.-C. Shen *et al.*, *Science* **268**, 1590 (1995).
5. R. Bennewitz *et al.*, *Surf. Sci.* **438**, 289 (1999).
6. J. Repp, G. Meyer, K.-H. Rieder, *Phys. Rev. Lett.* **92**, 036803 (2004).
7. Only the Cl^- ions are imaged as protrusions (*8*, *11*, *24*, *25*).
8. J. Repp, S. Fölsch, G. Meyer, K.-H. Rieder, *Phys. Rev. Lett.* **86**, 252 (2001).
9. G. Kresse, J. Furthmüller, *Phys. Rev. B* **54**, 11169 (1996).
10. G. Kresse, D. Joubert, *Phys. Rev. B* **59**, 1758 (1999).
11. F. E. Olsson, M. Persson, *Surf. Sci.* **540**, 172 (2003).
12. The vacuum region was 20 Å. The surface Brillouin zone was sampled by 2×2 *k*-points.
13. J. Tersoff, D. R. Hamann, *Phys. Rev. Lett.* **50**, 1998 (1983).
14. F. E. Olsson, M. Persson, N. Lorente, L. J. Lauhon, W. Ho, *J. Phys. Chem. B* **106**, 8161 (2002).
15. A. L. Shluger, A. M. Stoneham, *J. Phys. Condens. Matter* **5**, 3049 (1993).
16. M. Stoneham, P. W. Tasker, *J. Phys. C* **18**, L543 (1985).
17. The simulated STM images reproduce all features of the experimental appearance. However, a quantitative comparison of the images of Au^0 suffers from the limited ability of DFT to describe the NIR state by Kohn-Sham states.
18. G. P. Salam, M. Persson, R. E. Palmer, *Phys. Rev. B* **49**, 10655 (1994).
19. S. Gao, M. Persson, B. I. Lundqvist, *Solid State Commun.* **84**, 271 (1992).
20. C. Stipe *et al.*, *Phys. Rev. Lett.* **78**, 4410 (1997).
21. Note that $I(V)$ cannot be measured over this voltage range without immediately switching the Au adatom.
22. R. Bennewitz *et al.*, *Surf. Interface Anal.* **27**, 462 (1999).
23. A. Sanchez *et al.*, *J. Phys. Chem. A* **103**, 9573 (1999).
24. W. Hebenstreit *et al.*, *Surf. Sci.* **424**, L321 (1999).
25. F. E. Olsson, M. Persson, J. Repp, G. Meyer, http://arxiv.org/abs/cond-mat/0406282.
26. The intrinsic line width of the 6*s*-derived state could not be resolved, because the energy-level spacing is too large in the finite slab calculation.

27. We thank R. Allenspach for valuable comments and K.-H. Rieder for support. We acknowledge partial funding by the European Union projects "AMMIST" and "CHIC," the Swedish Research Council (VR), and the Swedish Strategic Foundation (SSF) through the materials consortium ATOMICS. Allocation of computer resources through the Swedish National Allocation Committee (SNAC) is also gratefully acknowledged.

23 April 2004; accepted 24 June 2004

Total Synthesis of Norzoanthamine

Masaaki Miyashita,* Minoru Sasaki, Izumi Hattori, Mio Sakai, Keiji Tanino

Norzoanthamine, an alkaloid isolated from *Zoanthus* sp., can suppress the loss of bone weight and strength in ovariectomized mice. Norzoanthamine derivatives can also strongly inhibit the growth of P-388 murine leukemia cell lines and human platelet aggregation. However, norzoanthamine's densely functionalized complex stereostructure and scarce availability from natural sources have proved a synthetic challenge. We report the stereoselective total synthesis of norzoanthamine in 41 steps, with an overall yield of 3.5% (an average of 92% yield each step).

The zoanthamine alkaloids, a type of heptacyclic marine alkaloid isolated from colonial zoanthids of the genus *Zoanthus* sp. (*1*–*11*), have attracted much attention from a wide area of science, including medicinal chemistry, pharmacology, natural product chemistry, and synthetic organic chemistry, because of their distinctive biological and pharmacological properties as well as their chemical structures with stereochemical complexity. For example, norzoanthamine (**1**), isolated by Uemura *et al.* in 1995 (*1*–*3*), can suppress the loss of bone weight and strength in ovariectomized mice and has been considered a promising candidate for an antiosteoporotic drug (*3*, *12*), whereas zoanthamine (**2**), isolated by Faulkner *et al.* (*4*, *5*), has exhibited potent inhibitory activity toward phorbol myristate–induced inflammation in addition to powerful analgesic effects (*5*, *6*). Very recently, norzoanthamine derivatives were demonstrated to inhibit strongly the growth of P-388 murine leukemia cell lines, in addition to their potent antiplatelet activities on human platelet aggregation (*13*). Thus, norzoanthamine (**1**) has been studied with keen interest, particularly in relation to the development of a new type of antiosteoporotic drug for use in those advanced in age (*3*, *12*). These distinctive biological properties, combined with novel chemical structures, make this family of alkaloids extremely attractive targets for chemical synthesis (Fig. 1).

However, the chemical synthesis of the zoanthamine alkaloids has remained as an unexplored summit, despite great synthetic efforts (*14*–*27*), owing to their densely functionalized complex stereostructures.

Synthetic challenges posed by norzoanthamine (**1**) and zoanthamine (**2**) include construction of the stereochemically dense C ring that has three adjacent quaternary asymmetric carbon atoms at the C-9, C-12, and C-22 positions; stereoselective synthesis of the ABC carbon framework consisting of the *trans-anti-trans*-fused perhydrophenanthren skeleton; and stereoselective construction of two novel aminoacetal structures, including a bridged δ-lactone.

Division of Chemistry, Graduate School of Science, Hokkaido University, Sapporo 060-0810, Japan.

*To whom correspondence should be addressed. E-mail: miyasita@sci.hokudai.ac.jp

We set about synthetic studies of norzoanthamine (**1**) that aimed at developing an efficient synthetic route flexible enough to provide access to several members of the zoanthamine alkaloids while allowing the synthesis of various analogs for biological testing. We report herein the stereoselective total synthesis of **1.**

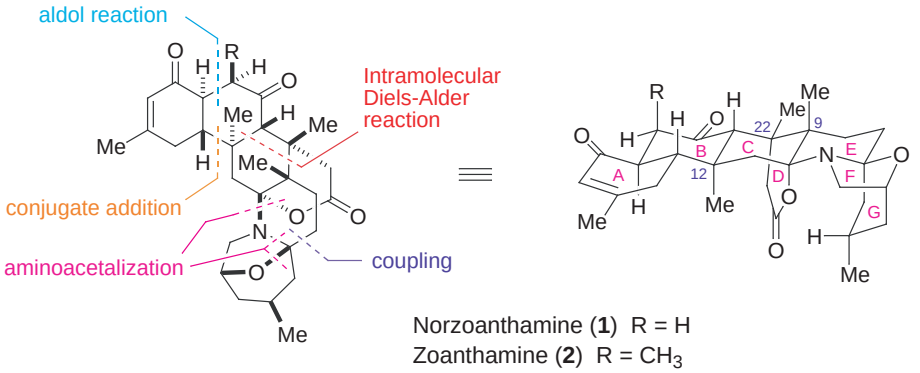

Fig. 1. Molecular structures of norzoanthamine (**1**) and zoanthamine (**2**) and retrosynthesis of norzoanthamine (**1**).

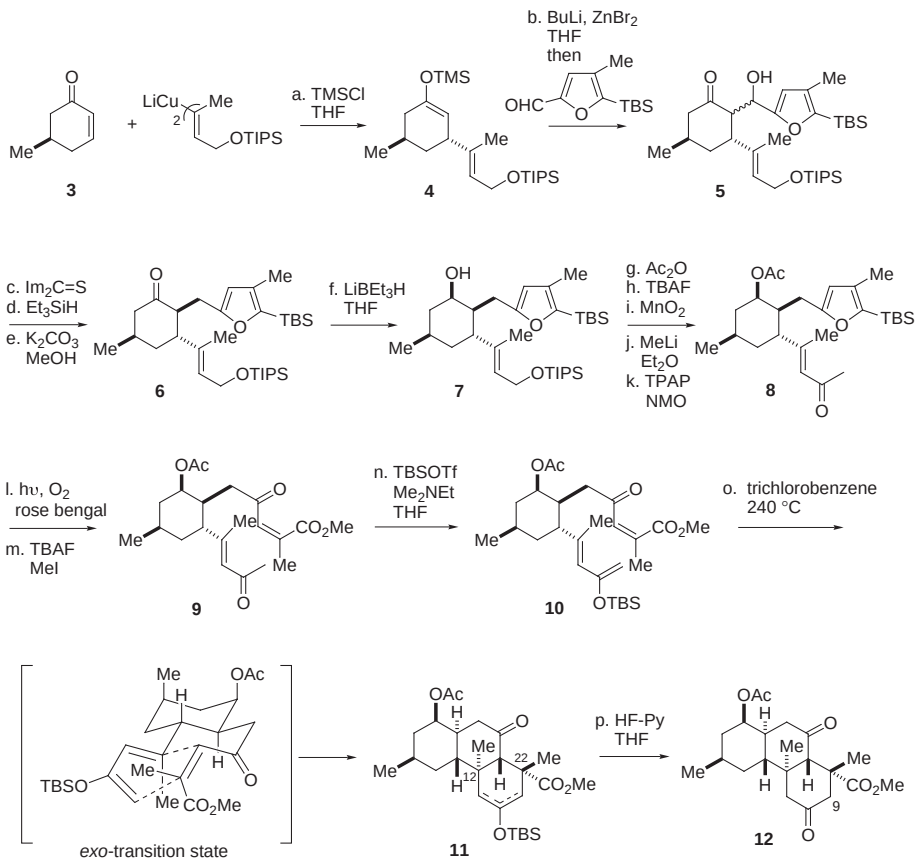

Fig. 2. Synthesis of the ABC ring system **12**. Reagents and conditions are as follows: (**a**) chlorotrimethylsilane (TMSCl), tetrahydrofuran (THF), −40°C, 1 hour; (**b**) butyllithium (BuLi), THF, −30°C, 2 hours, $ZnBr_2$, −78°C, 2 hours, then 4-methyl-5-[*tert*-butyldimethylsilyl]furfural, −78°C, 3 hours, 84% (two steps); (**c**) 1,1′-thiocarbonyldiimidazole ($Im_2C{=}S$), toluene, 70 to 90°C, 6.5 hours, 92%; (**d**) triethylsilane (Et_3SiH), chlorotris(triphenylphosphine)rhodium(I), THF, 50°C, 2 hours; (**e**) K_2CO_3, methanol (MeOH), THF, room temperature (RT), 1 hour, 86% (two steps); (**f**) lithium triethylborohydride ($LiBEt_3H$), THF, −78°C, 30 min, 98%; (**g**) acetic anhydride (Ac_2O), pyridine, 4-dimethylaminopyridine, dichloromethane (CH_2Cl_2), RT, 1.5 hours; (**h**) tetra-*n*-butylammonium fluoride (TBAF), THF, RT, 5 hours, 96% (two steps); (**i**) manganese(IV) oxide (MnO_2), CH_2Cl_2, RT, 13 hours; (**j**) methyllithium (MeLi), ether (Et_2O), −100°C, 3 hours; (**k**) tetrapropylammonium perruthenate (TPAP), 4-methylmorpholine-*N*-oxide (NMO), molecular sieves 4A, CH_2Cl_2, RT, 1.5 hours, 95% (three steps); (**l**) halogen lamp (hυ), rose bengal, oxygen (O_2), CH_2Cl_2, 0°C, 12 hours; (**m**) TBAF, iodomethane (MeI), THF, RT, 1 hour, 97% (two steps); (**n**) *tert*-butyldimethylsilyl trifluoromethanesulfonate (TBSOTf), *N*,*N*-dimethylethylamine (Me_2NEt), CH_2Cl_2, 0°C, 30 min, 100%; (**o**) 1,2,4-trichlorobenzene, 240°C, 1.5 hours; (**p**) hydrogen fluoride-pyridine (HF-Py), THF, RT, 3 hours, 51% (two steps).

In the synthetic direction, the following key operations were proposed: (i) stereoselective construction of the DEFG ring system by bis-aminoacetalization of the precursor keto carboxylic acid bearing an amino-alcohol side chain; (ii) construction of the ABC ring system, including two quaternary asymmetric carbon centers at the C-12 and C-22 positions, through an intramolecular Diels-Alder reaction (*27*), which was designed by taking into account the proposed biogenetic pathway for the zoanthamine alkaloids (*3*); and (iii) stereospecific synthesis of the requisite triene for the key Diels-Alder reaction by the three-component coupling reactions, which involve a conjugate addition of a vinylcupurate reagent followed by an aldol reaction and subsequent photosensitized oxidation of a furan ring.

Our first objective focused on the stereoselective synthesis of the key precursor for the intramolecular Diels-Alder reaction by the three-component coupling reactions. Figure 2 presents the synthesis of the requisite triene **10** starting from (*R*)-5-methylcyclohexenone (**3**) (*28*). Conjugate addition of lithium bis[(*E*)-1-methyl-3-(triisopropylsilyloxy)-1-propenyl]cupurate (*27*) to (*R*)-5-methylcyclohexenone (**3**) in tetrahydrofuran (THF) in the presence of chlorotrimethylsilane (TMSCl) (*29*) provided silyl enol ether **4** stereoselectively, which was subjected to the aldol reaction with the functionalized furaldehyde (*27*) by means of zinc enolate to give aldol **5** as a diastereoisomeric mixture (84% yield, two steps). As we expected, the conjugate addition of the vinylcupurate exclusively occurred from the opposite side of the secondary methyl group on the cyclohexene ring. After dehydration of the aldols **5** with 1,1′-thiocarbonyldiimidazole, the resulting enones (*E*/*Z* = 96:4) were subjected to the hydrosilylation reaction in the presence of Wilkinson's catalyst (*30*). Subsequent treatment of the silyl enol ether with K_2CO_3 in methanol (MeOH) furnished the trisubstituted cyclohexanone **6** with the desired stereochemistry (79% yield, three steps). Reduction of **6** with lithium triethylborohydride ($LiBEt_3H$) in THF afforded the single β-alcohol **7** quantitatively. Then, **7** was converted to methyl ketone **8** by a routine five-step reaction sequence: (i) acetylation, (ii) removal of the triisopropylsilyl (TIPS) group, (iii) oxidation with manganese dioxide (MnO_2), (iv) addition of methyllithium (MeLi) to aldehyde, and (v) oxidation of the secondary alcohol with tetrapropylammonium perruthenate (TPAP) in 91% overall yield.

The next crucial photosensitized oxidation of the furan **8** was successfully performed according to the Katsumura protocol with a halogen lamp and rose bengal (*31*) to afford the desired *Z*-γ-keto-α,β-unsaturated silyl ester quantitatively, which was immediately converted to the stable

methyl ester **9** using tetrabutylammonium fluoride (TBAF) and iodomethane (MeI) in THF (*32*) in 97% yield (two steps). The requisite triene **10** was synthesized by treatment of **9** with *tert*-butyldimethylsilyl trifluoromethanesulfonate (TBSOTf) and *N,N*-dimethylethylamine (Me_2NEt) in THF.

The next step was the crucial intramolecular Diels-Alder reaction. As shown in Fig. 2, this reaction proceeded with high efficiency by adding dropwise a solution of **10** in 1,2,4-trichlorobenzene into the same solvent heated at 240°C, which gave rise to a 72:28 mixture of the exo and the endo adducts, respectively, in 98% combined yield. When the adducts were treated with hydrogen fluoride (HF)–pyridine, the major crystalline compound **12** was readily obtainable by simple crystallization in 51% isolated yield. The stereostructure of **12** was unambiguously confirmed by x-ray crystallographic analysis and determined to be that of the exo adduct. Thus, the intramolecular Diels-Alder reaction of **10** occurred stereoselectively through the exo transition state, as we expected, to give rise to the ABC ring system with two quaternary asymmetric carbon centers at the C-12 and C-22 positions. At this stage, the total yield of **12** from 5-methylcyclohexenone (**3**) was remarkably high, 29% in 16 steps.

We focused next on the construction of another quaternary asymmetric carbon center at the C-9 position. To construct this particular stereogenic center stereoselectively, we designed the synthetic route shown in Fig. 3, which involved an intramolecular acylation reaction of keto alcohol **16** and a subsequent C-methylation reaction of the resulting keto lactone as the key steps. **12** was converted to hydroxy lactone **13** in a highly stereoselective manner by treatment with potassium tri-*sec*-butylborohydride (K-Selectride) in THF and CH_2Cl_2 (82% yield), which was transformed into **14** by a three-step reaction sequence: (i) protection of the secondary alcohol with a *tert*-butyldimethylsilyl (TBS) group; (ii) removal of the acetate; and (iii) protection of the hydroxyl group in the A-ring with a triethylsilyl (TES) group (90%, three steps). Reduction of **14** with diisobutylaluminum hydride (DIBAL) in toluene followed by the Wittig reaction of the resultant lactol with methyl-*d*3-triphenylphosphonium bromide (Ph_3PCD_3Br) furnished vinyl derivative, which was then subjected to hydroboration with 9-borabicyclo[3.3.1]nonane (9-BBN) to afford diol **15** in high yield. Chemoselective oxidation of the secondary alcohol in **15** was performed by the Trost protocol, using ammonium molybdate $[(NH_4)_6Mo_7O_{24}{\cdot}4H_2O]$ and hydrogen peroxide (H_2O_2) (*33*), giving rise to the keto alcohol **16** in 90% yield.

With the synthetic intermediate **16** in hand, we focused on the stereoselective construction of the quaternary asymmetric carbon center at the C-9 position. The key conversion was realized as follows. Upon treatment of **16** with dimethyl carbonate $[(MeO)_2C{=}O]$ and lithium *tert*-butoxide (*t*BuOLi) in THF and hexamethylphosphoramide (HMPA) at 75°C, formation of carbonate and subsequent intramolecular acylation reaction smoothly occurred to form the lithium enolate of β-keto lactone, which was reacted with iodomethane (MeI) to give methyl enol ether **17** as a single product in 92% yield.

Further treatment of **17** with *t*BuOLi in THF and 1,3-dimethyl-3,4,5,6-tetrahydro-2(1*H*)-pyrimidinone (DMPU), followed by an addition of MeI, produced the targeted compound **18** as a single stereoisomer in 83% yield, in which a new methyl group was highly stereoselectively introduced from the β side at the C-9 position. The crucial alkyne segment **20** was derived from **18** by a three-step reaction sequence: addition of methyllithium (MeLi), protection of the resulting primary alcohol with a TBS group leading to **19** (88%, two steps), and formation of enol trifluoromethanesulfonate and subsequent elimination with diazabicyclo[5.4.0]undec-7-ene (DBU) (81%). Thus, the requisite alkyne segment **20** was efficiently synthesized by exploiting a deuterium kinetic isotope effect: Nondeuterated methyl ketone resulted in the formation of a considerable amount of byproduct (nondeuterated **21**, 30%) along with the desired alkyne (nondeuterated **20**, 66%). The mechanistic analysis that the nondeuterated **21** was formed by a 1,5-hydride shift from nondeuterated **19**, as shown in **21**$^{\neq}$, led us to use a deuterium kinetic isotope effect

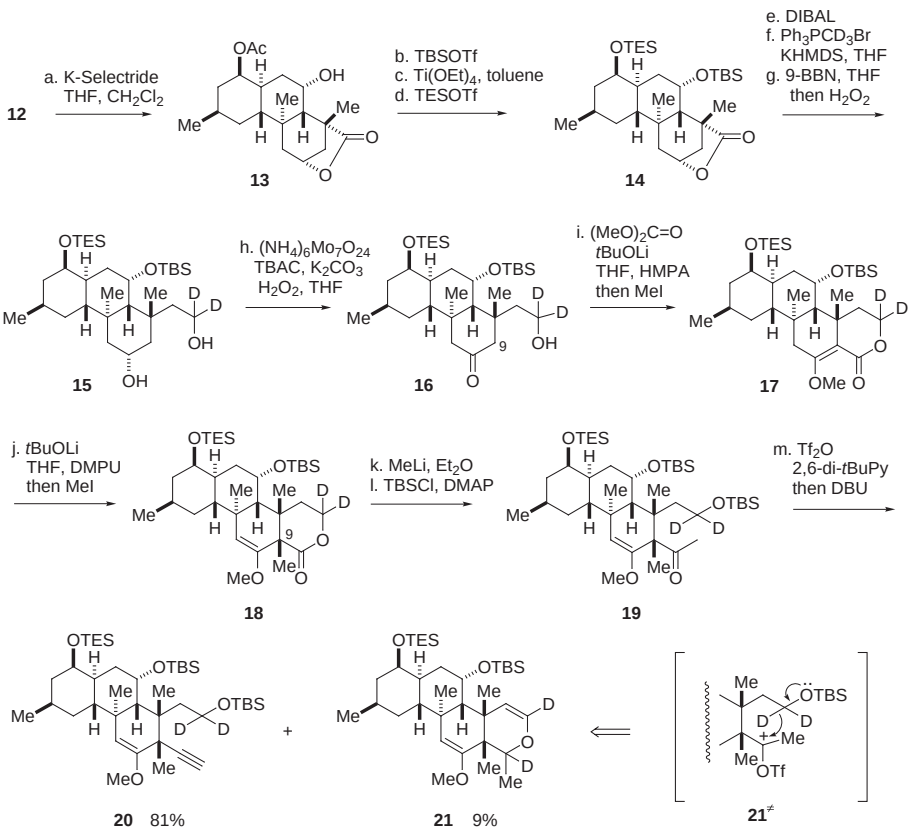

Fig. 3. Synthesis of the alkyne segment **20** by the use of deuterium. Reagents and conditions are as follows: (**a**) potassium tri-*sec*-butylborohydride (K-Selectride), THF, CH_2Cl_2, –78°C, then –10°C, 11 hours; (**b**) *tert*-butyldimethylsilyl trifluoromethanesulfonate (TBSOTf), 2,6-lutidine, CH_2Cl_2, RT, 4 hours, 82% (two steps); (**c**) titanium(IV) ethoxide $[Ti(OEt)_4]$, toluene, 100°C, 24 hours; (**d**) triethylsilyl trifluoromethanesulfonate (TESOTf), 2,6-lutidine, CH_2Cl_2, 0°C, 1 hour, 90% (two steps); (**e**) diisobutylaluminum hydride (DIBAL), toluene, –78°C, 2 hours, 85% (repeated three times); (**f**) methyl-d_3-triphenylphosphonium bromide (Ph_3PCD_3Br), potassium hexamethyldisilazide (KHMDS), THF, 0°C, 2 hours; (**g**) 9-borabicyclo[3.3.1]nonane (9-BBN), THF, 80°C, 1 hour, then hydrogen peroxide (H_2O_2), RT, 12 hours; (**h**) ammonium molybdate $[(NH_4)_6Mo_7O_{24}{\cdot}4H_2O]$, tetrabutylammonium chloride (TBAC), K_2CO_3, H_2O_2, THF, RT, then 50°C, 7 hours, 90% (three steps); (**i**) dimethyl carbonate $[(MeO)_2C{=}O]$, lithium *tert*-butoxide (*t*BuOLi), hexamethylphosphoramide (HMPA), THF, 75°C, 4 hours, then iodomethane (MeI), RT, 2 hours, 92%; (**j**) *t*BuOLi, 1,3-dimethyl-3,4,5,6-tetrahydro-2(1*H*)-pyrimidinone (DMPU), THF, 0°C to RT, 1 hour, then MeI, RT, 2 hours, 83%; (**k**) methyllithium (MeLi), ether (Et_2O), 0°C, 1 hour; (**l**) *tert*-butyldimethylsilyl chloride (TBSCl), triethylamine (Et_3N), 4-dimethylaminopyridine (DMAP), *N,N*-dimethylformamide (DMF), RT, 3 hours, 88% (two steps); (**m**) trifluoromethanesulfonic anhydride (Tf_2O), 2,6-di-*tert*-butylpyridine (2,6-di-*t*BuPy), dichloroethane $[(CH_2Cl)_2]$, RT, 3 hours, then diazabicyclo[5.4.0]undec-7-ene (DBU), 80°C, 3 hours, 81%.

for this particular alkynylation reaction to suppress the formation of **21**. Indeed, the formation of **21** was suppressed less than 9% through this isotope effect (*34*).

The amino-alcohol fragment **22** was synthesized starting from (*R*)-citroneral by means of the Jacobsen kinetic resolution protocol (*35*). With the key alkyne segment **20** and the amino-alcohol segment **22** in hand, we then needed to couple the two segments, install a double bond into the A-ring, and perform the final bis-aminoacetalization to form the DEFG ring framework (Fig. 4).

The coupling reaction of **20** and **22** with butyllithium (BuLi) in THF, followed by oxidation of the adducts with 1,1,1-triacetoxy-1,1-dihydro-1,2-benziodoxol-3(1*H*)-one (DMP), afforded **23** in 82% yield. Alkynyl ketone **23** was then converted to the crucial keto acid **26** by the following reaction sequence: (i) hydrogenation of the triple bond; (ii) treatment with aqueous acetic acid (AcOH) at 50°C, leading to aminoacetal **24**; (iii) removal of two *tert*-butyldimethylsilyl (TBS) groups with tetrabutylammonium fluoride (TBAF); (iv) selective oxidation of secondary hydroxyl groups with ammonium molybdate [$(NH_4)_6Mo_7O_{24}{\cdot}4H_2O$] to derive **25**; (v) oxidation of the primary alcohol to aldehyde with tetrapropylammonium perruthenate (TPAP); and (vi) sodium chlorite ($NaClO_2$) oxidation of the aldehyde to the carboxylic acid **26** (61% yield from **23**).

Regioselective introduction of a double bond into the A ring was successfully performed by using the Ito-Saegusa method (*36*). Esterification of **26** with (trimethylsilyl)diazomethane ($TMSCHN_2$) in CH_2Cl_2, followed by treatment with chlorotrimethylsilane (TMSCl) and lithium hexamethyldisilazide (LHMDS) in THF, solely produced trimethylsilyl enol ether of the ketone in the A ring. Reaction with palladium acetate [$Pd(OAc)_2$] in acetonitrile (CH_3CN) furnished the desired enone **27** in 96% yield for the three steps.

The final critical bis-aminoacetalization, i.e., the construction of the DEFG rings culminating in the total synthesis of norzoanthamine, was achieved by initial treatment of **27** with aqueous acetic acid (AcOH) at 100°C, followed by treatment of the resulting iminium salt **28** with aqueous trifluoroacetic acid (TFA) at 110°C to produce the ammonium salts of norzoanthamine **29**. Finally, desalination of **29** with basic alumina in MeOH furnished norzoanthamine in 81% yield (three steps). The total yield of synthetic norzoanthamine was 3.5% (an average of 92% yield each step) in 41 steps, starting from **3**. The synthetic compound was identical in all respects with naturally occurring norzoanthamine, including spectroscopic characteristics [^1H and ^{13}C nuclear magnetic resonance (NMR) spectra, infrared spectroscopy, and mass spectra], circular dichroism (CD) (*37*), and optical rotation [$(\alpha)^{24}_D$ −6.0 (*c* 0.23, $CHCl_3$); natural norzoanthamine: $(\alpha)^{24}_D$ −6.2 (*c* 0.23, $CHCl_3$)] (*38*).

The absolute structure of norzoanthamine (**1**) was rigorously verified by the present total synthesis. The chemistry described here not only offers a solution to a formidable synthetic challenge but also opens a completely chemical avenue to norzoanthamine, other naturally occurring zoanthamine alkaloids, and synthetic, designed norzoanthamine derivatives.

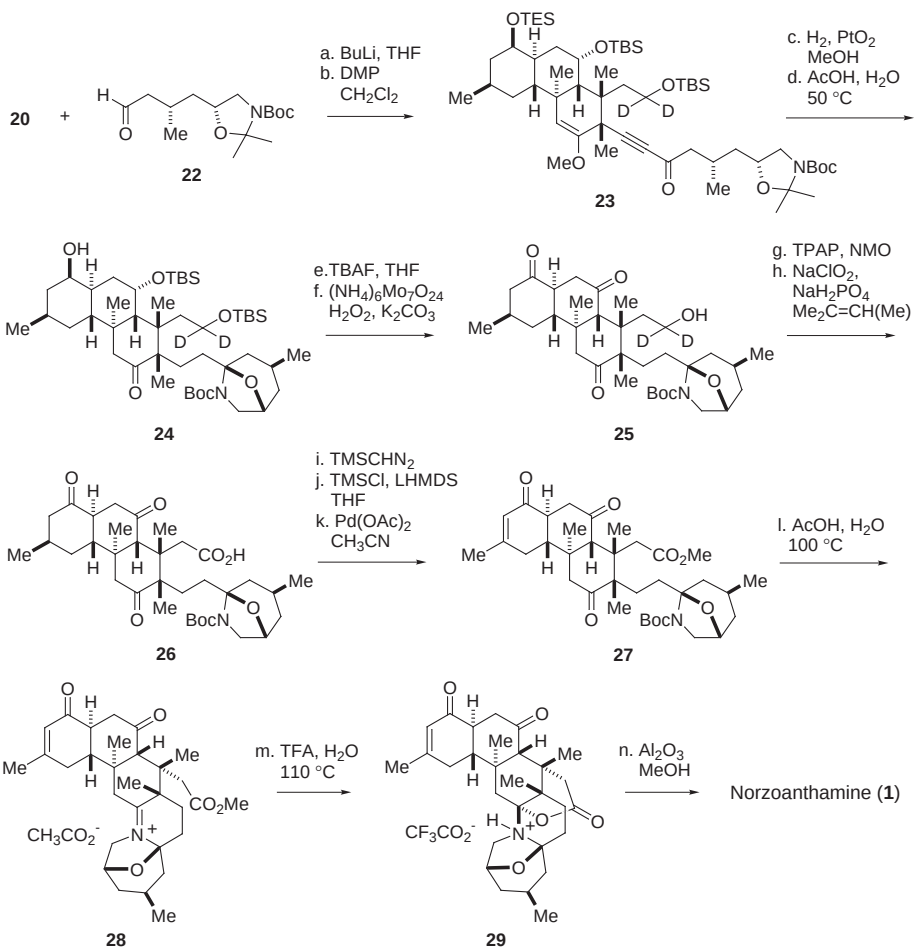

Fig. 4. Total synthesis of norzoanthamine (**1**). Reagents and conditions are as follows: (**a**) butyllithium (BuLi), THF, –30°C, 30 min, then **22**, –78°C, 1 hour; (**b**) 1,1,1-triacetoxy-1,1-dihydro-1,2-benziodoxol-3(1*H*)-one (DMP), pyridine, CH_2Cl_2, RT, 2 hours, 82% (two steps); (**c**) H_2, platinum(IV) oxide (PtO_2), MeOH, RT, 8 hours; (**d**) acetic acid (AcOH), H_2O, 50°C, 5 hours; (**e**) tetra-*n*-butylammonium fluoride (TBAF), THF, 70°C, 2 hours; (**f**) ammonium molybdate [$(NH_4)_6Mo_7O_{24}{\cdot}4H_2O$], K_2CO_3, hydrogen peroxide (H_2O_2), THF, 50°C, 3 hours; (**g**) tetrapropylammonium perruthenate (TPAP), 4-methylmorpholine-*N*-oxide (NMO), molecular sieves 4A, CH_2Cl_2, RT, 1 hour; (**h**) sodium chlorite ($NaClO_2$), sodium dihydrogenphosphate (NaH_2PO_4), 2-methyl-2-butene [$Me_2C{=}CH(Me)$], H_2O, *tert*-butanol (*t*BuOH), RT, 1 hour, 61% from **23**; (**i**) (trimethylsilyl)diazomethane ($TMSCHN_2$), MeOH, CH_2Cl_2, RT, 1 hour; (**j**) chlorotrimethylsilane (TMSCl), lithium hexamethyldisilazide (LHMDS), THF, –65°C, 1 hour; (**k**) palladium(II) acetate [$Pd(OAc)_2$], acetonitrile (CH_3CN), 50°C, 2 hours, 96% (three steps); (**l**) AcOH, H_2O, 100°C, 24 hours; (**m**) trifluoroacetic acid (TFA), H_2O, 110°C, 24 hours; (**n**) basic aluminum oxide (Al_2O_3), MeOH, RT, 1 hour, 81% from **27**.

References and Notes

1. S. Fukuzawa *et al.*, *Heterocycl. Commun.* **1**, 207 (1995).
2. M. Kuramoto *et al.*, *Tetrahedron Lett.* **38**, 5683 (1997).
3. M. Kuramoto *et al.*, *Bull. Chem. Soc. Jpn.* **71**, 771 (1998).
4. C. B. Rao *et al.*, *J. Am. Chem. Soc.* **106**, 7983 (1984).
5. C. B. Rao *et al.*, *J. Org. Chem.* **50**, 3757 (1985).
6. C. B. Rao, D. V. Rao, V. S. N. Raju, *Heterocycles* **28**, 103 (1989).
7. A. Rahman, K. A. Alvi, S. A. Abbas, M. I. Choudhary, J. Clardy, *Tetrahedron Lett.* **30**, 6825 (1989).
8. A. H. Daranas, J. J. Fernández, J. A. Gavín, M. Norte, *Tetrahedron* **54**, 7891 (1998).
9. H. Nakamura, Y. Kawase, K. Maruyama, A. Murai, *Bull. Chem. Soc. Jpn.* **71**, 781 (1998).
10. Y. Venkateswarlu, N. S. Reddy, P. Ramesh, P. S. Reddy, K. Jamil, *Heterocycl. Commun.* **4**, 575 (1998).
11. A. H. Daranas, J. J. Fernández, J. A. Gavín, M. Norte, *Tetrahedron* **55**, 5539 (1999).
12. K. Yamaguchi, M. Yada, T. Tsuji, M. Kuramoto, D. Uemura, *Biol. Pharm. Bull.* **22**, 920 (1999).
13. R. M. Villar *et al.*, *Bioorg. Med. Chem.* **11**, 2301 (2003).

14. D. Tanner, P. G. Andersson, L. Tedenborg, P. Somfai, *Tetrahedron* **50**, 9135 (1994).
15. D. Tanner, L. Tedenborg, P. Somfai, *Acta Chem. Scand. A* **51**, 1217 (1997).
16. T. E. Nielsen, D. Tanner, *J. Org. Chem.* **67**, 6366 (2002).
17. D. R. Williams, G. S. Cortez, *Tetrahedron Lett.* **39**, 2675 (1998).
18. D. R. Williams, T. A. Brugel, *Org. Lett.* **2**, 1023 (2000).
19. S. Ghosh, F. Rivas, D. Fischer, M. A. González, E. A. Theodorakis, *Org. Lett.* **6**, 941 (2004).
20. G. Hirai, H. Oguri, M. Hirama, *Chem. Lett.* **28**, 141 (1999).
21. S. M. Moharram, G. Hirai, K. Koyama, H. Oguri, M. Hirama, *Tetrahedron Lett.* **41**, 6669 (2000).
22. G. Hirai, H. Oguri, S. M. Moharram, K. Koyama, M. Hirama, *Tetrahedron Lett.* **42**, 5783 (2001).
23. G. Hirai, Y. Koizumi, S. M. Moharram, H. Oguri, M. Hirama, *Org. Lett.* **4**, 1627 (2002).
24. N. Hikage, H. Furukawa, K. Takao, S. Kobayashi, *Tetrahedron Lett.* **39**, 6237 (1998).
25. N. Hikage, H. Furukawa, K. Takao, S. Kobayashi, *Tetrahedron Lett.* **39**, 6241 (1998).
26. N. Hikage, H. Furukawa, K. Takao, S. Kobayashi, *Chem. Pharm. Bull. (Tokyo)* **48**, 1370 (2000).
27. M. Sakai, M. Sasaki, K. Tanino, M. Miyashita, *Tetrahedron Lett.* **43**, 1705 (2002).
28. S. Mutti, C. Daubié, F. Decalogne, R. Fournier, P. Rossi, *Tetrahedron Lett.* **37**, 3125 (1996).
29. E. Nakamura, S. Matsuzawa, Y. Horiguchi, I. Kuwajima, *Tetrahedron Lett.* **27**, 4029 (1986).
30. I. Ojima, T. Kogure, *Organometallics* **1**, 1390 (1982).
31. S. Katsumura, K. Hori, S. Fujiwara, S. Isoe, *Tetrahedron Lett.* **38**, 4625 (1985).
32. T. Ooi, H. Sugimoto, K. Maruoka, *Heterocycles* **54**, 593 (2001).
33. B. M. Trost, Y. Masuyama, *Tetrahedron Lett.* **25**, 173 (1984).
34. The use of deuterium isotope effects in natural product synthesis. See (*39*–*41*).
35. H. Lebel, E. N. Jacobsen, *Tetrahedron Lett.* **40**, 7303 (1999).
36. Y. Ito, T. Hirao, T. Saegusa, *J. Org. Chem.* **43**, 1011 (1978).
37. Selected physical data, ^{1}H-NMR and ^{13}C-NMR spectra, mass spectra, and CD spectra are provided as supporting material on *Science* Online.
38. The optical rotation of natural norzoanthamine showed $[\alpha]^{24}_D$ −6.2 (*c* 0.23, $CHCl_3$), contrary to the reported value $[\alpha]_D$ +1.6 (*c* 0.42, $CHCl_3$) (*1*, *3*).
39. D. L. J. Clive, M. Cantin, A. Khodabocus, X. Kong, Y. Tao, *Tetrahedron* **49**, 7917 (1993).
40. D. L. J. Clive *et al.*, *J. Am. Chem. Soc.* **116**, 11275 (1994).
41. E. Vedejs, J. Little, *J. Am. Chem. Soc.* **124**, 748 (2002).
42. We are grateful to D. Uemura for providing us with natural norzoanthamine. Financial support from the Ministry of Education, Culture, Sports, Science, and Technology, Japan [a Grant-in-Aid for Scientific Research (A) (No. 12304042) and a Grant-in-Aid for Scientific Research on Priority Areas (A) "Exploitation of Multi-Element Cyclic Molecules" (No. 13029003)] is gratefully acknowledged.

Supporting Online Material
www.sciencemag.org/cgi/content/full/1098851/DC1
SOM Text
Figs. S1 to S4

6 April 2004; accepted 2 June 2004
Published online 17 June 2004;
10.1126/science.1098851
Include this information when citing this paper.

Rapid Late Pleistocene Incision of Atlantic Passive-Margin River Gorges

Luke J. Reusser,[1]* Paul R. Bierman,[1] Milan J. Pavich,[2] E-an Zen,[3] Jennifer Larsen,[1] Robert Finkel[4]

The direct and secondary effects of rapidly changing climate caused large rivers draining the Atlantic passive margin to incise quickly into bedrock beginning about 35,000 years ago. Measured in samples from bedrock fluvial terraces, 10-beryllium shows that both the Susquehanna and Potomac Rivers incised 10- to 20-meter-deep gorges along steep, convex lower reaches during the last glacial cycle. This short-lived pulse of unusually rapid downcutting ended by 13,000 to 14,000 years ago. The timing and rate of downcutting are similar on the glaciated Susquehanna and unglaciated Potomac Rivers, indicating that regional changes, not simply glacial meltwater, initiated incision.

A fundamental control on the development of landscapes is the rate at which rivers cut through rock. River incision into bedrock translates the effects of climate and tectonics through drainage networks, thus controlling rates of landscape evolution (*1*, *2*). Despite broad interest in understanding the style and timing of landscape change, only a handful of studies have directly measured the rate and timing of fluvial bedrock incision. Most of these studies quantifying bedrock incision rates have been conducted in tectonically active regions (*3*–*5*); however, the majority of Earth's surface is tectonically quiescent, including passive margins around the globe for which river incision rates are largely unknown. In this report, we used 59 measurements of cosmogenic ^{10}Be (tables S1 and S2) to quantify the rate and timing of bedrock incision along two of the largest rivers draining the Atlantic passive margin, the Susquehanna (70,200 km^2) and the Potomac (29,900 km^2) (Fig. 1).

Over millions of years, large rivers draining the Atlantic passive margin have carved broad valleys into rocks of the Appalachian Piedmont, where river profiles are convex along their lower reaches (Fig. 2, C and D) (*6*–*8*). Long-term gradual lowering of the Susquehanna and Potomac Valleys [~0.01 to 0.02 meters per thousand years (m/ky)] into the Piedmont uplands reflects a combination of slow flexural uplift of the Atlantic margin from offshore sediment loading, isostatic response to denudation, and protracted late Cenozoic sea-level fall (*7*–*9*). Within these broad valleys are narrow gorges, bounded by bare-rock terraces.

The Susquehanna River narrows and deepens in its lower reaches, passing through a series of bedrock gorges. Holtwood, the largest gorge, is about 5 km long, 1 km wide, and incised into a broad valley set nearly 150 m into the Piedmont uplands. This gorge contains three distinct levels of bedrock terraces (Fig. 2A) as well as weathered high points representing remnants of older, degraded levels. The northern half of the Susquehanna Basin has been glaciated repeatedly (*10*); thus, glacial meltwater and sediment passed down the Susquehanna channel and through Holtwood Gorge.

Similarly, the Potomac River lies more than 100 m below the uplands within a broad outer valley. The river drops nearly 20 m as it passes over Great Falls and through 3-km-long Mather Gorge. The gorge is 75 to 125 m wide (*11*) and confined by a 1-km-wide bedrock terrace (Fig. 2B). This terrace is studded with fluvially rounded outcrops standing decimeters to meters above the bedrock surface. The Potomac Basin remained glacier-free during the Pleistocene (*10*).

We sampled fluvially eroded bedrock surfaces exposed as these rivers incised toward younger and lower levels. Most outcrops preserved distinct fluvial forms, suggesting little erosion since abandonment and exposure (*12*). Modeling suggests that ^{10}Be ages are not substantially affected by floodwater absorption of cosmic rays (*13*), and no sediment covers the outcrops today. Rapid incision and the low ^{10}Be content of samples collected from the modern bank of the Potomac River (*14*) allow us to model ^{10}Be concentrations directly as terrace abandonment ages.

[1]Department of Geology and School of Natural Resources, University of Vermont, Burlington, VT 05401, USA. [2]U.S. Geological Survey (USGS), National Center, Reston, VA 20192, USA. [3]Department of Geology, University of Maryland, College Park, MD 20742, USA. [4]Center for Accelerator Mass Spectrometry, Lawrence Livermore National Laboratory, Livermore, CA 94550, USA.

*To whom correspondence should be addressed. E-mail: lreusser@uvm.edu

Total Synthesis of Norzoanthamine

Masaaki Miyashita, Minoru Sasaki, Izumi Hattori, Mio Sakai and Keiji Tanino (June 17, 2004)

Science **305** (5683), 495-499. [doi: 10.1126/science.1098851]
originally published online June 17, 2004